3D Shear layer model for the simulation of multiple wind turbine wakes: Description and first assessment

Davide Trabucchi, Lukas Vollmer, and Martin Kühn

ForWind - University of Oldenburg, Institute of Physics, Küpkersweg, 70, 26129 Oldenburg, Germany

Correspondence to: Davide Trabucchi (davide.trabucchi@uni-oldenburg.de)

Abstract. The number of turbines installed in offshore wind farms has strongly increased in the last years and at the same time the need for more precise estimation of the wind farm efficiency too. In this sense, the interaction between wakes has become a relevant aspect for the definition of a wind farm layout, for the assessment of its annual energy yield and for the evaluation of wind turbine fatigue loads. For this reason, accurate models for multiple wakes are a main concern of the wind energy community. Existing engineering models can only simulate single wakes which are superimposed when they are interacting in a wind farm. This method is a practical solution, but it is not fully supported by a physical background. The limitation to single wakes is given by the assumption that the wake is axisymmetric. As alternative, we propose a new shear layer model which is based on the existing engineering wake models, but is extended to simulate also non-axisymmetric wakes. In this paper, we present the theoretical background of the model and four application cases. We evaluate the new model for the simulation of single and multiple wakes using large eddy simulations as reference. In particular, we report the improvements of the new model predictions in comparison to a sum-of-squares superposition approach for the simulation of three interacting wakes. The lower deviation from the reference considering single and multiple wakes encourages the further development of the model and promises a successful application for the simulation of wind farms.

1 Introduction

When the wind passes through the wind turbine rotor, kinetic energy is extracted from the wind and is converted into electrical power. The reduced kinetic energy is revealed by a wake deficit behind the rotor, i.e. a shear flow with lower speed and higher turbulent fluctuations than in the free flow upstream and sideways.

In this sense, wakes are the main cause of power losses in wind farms (Walker et al., 2016). Besides that, wakes hitting a turbine contribute to the increase in the fatigue loads of its components. For these reasons, wake modeling plays a major role in the definition of the layout of wind farms, in the evaluation of their annual energy yield and in the estimation of the lifetime of wind turbine components. Consequently, more accurate wake models can indirectly contribute to the cost-of-energy reduction thanks to more tailored design of wind turbines and wind farms.

Despite the large progress especially in the numerical modelling, Vermeer et al. (2003) still provide a comprehensive review about traditional wake modeling. Most of the engineering models described in their work evaluate the wind field of a single wake and combine the individual results in case of mutual interaction. More sophisticated Computational Fluid Dynamics
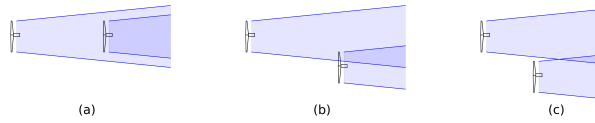
Figure 1. Different cases of merging wakes: (a) Aligned wakes (b) Wake-turbine interaction (c) Wake-wake interaction.

(CFD) such as Reynolds averaged Navier-Stokes (RANS) or large eddy simulations (LES) can provide more realistic results because the physics of the flow is resolved up to more refined length and time scales. However, these alternatives have a much higher computational cost and therefore can become prohibitive for design applications.

Engineering tools for estimating wake effects in a wind farm often implement the steady state, axisymmetric shear layer approximation of the RANS equations, e.g. the one used in the Ainslie model (Ainslie, 1988). Due to the axial symmetry assumption, only the wind deficit of single wakes or wakes aligned on the same axis as those illustrated in Fig. 1a can be simulated with such models. For the case of wake-turbine or wake-wake interaction of Fig. 1b and c pragmatic methods are required. In the kinematic model by Katic et al. (1986), the square addition of the individual wake deficits is applied to deal with multiple wakes. In a previous study, Lissaman (1979) proposed the linear addition of the wake deficits, however this method tends to overestimate the velocity deficit and could lead to unrealistic flow reversal when many wakes merge.

Machefaux (2015) compared the performance of the linear approach with the one of the square wake addition approach and noticed that the former is to be preferred for wakes of turbines operating at a low thrust coefficients, while the latter returns better results in the opposite case. From this observation, he developed a wake superposition model which combines the linear and square addition of single wakes using a weighted average depending on the thrust on the rotor.

Crespo et al. (1999) declared that the classical wake superposition methods do not rely on a physical background and, if not handled properly, could lead to unrealistic results. This statement gives the motivation of this paper. In this regard, we aim to investigate whether a more detailed physical model could improve the simulation of multiple wakes. For this purpose, we picked up the suggestion by Ainslie (1988) to extend his model to the third dimension, dropping the hypothesis of an axisymmetric wake profile; accordingly, we developed the 3D shear layer (3DSL) model and tested its performances in relation to Ainslie's model and the square addition approach. For the assessment, we addressed four cases including a single wake, aligned wakes, wake-turbine and wake-wake interaction; we used the wind fields extracted from LES of the same wake conditions as reference and considered the section average wind speed and the root mean square error as figures of merit.

2 Model description

In the following the theoretical background of the 3DSL model is provided along with the description of its numerical implementation. Moreover, it is explained how to evaluate the parameters needed to apply the model.

2.1 The mathematical definition

The 3DSL model is meant to add the third dimension to the shear layer approximation of the steady RANS equations for wind turbine wake simulations first described by Ainslie (1988), maintaining all his assumptions but the one of an axisymmetric wake profile. The 3DSL model is intended to simulate the downstream development of the wind turbine wake deficit u_D defined as

$$u_D(x,y,z) = 1 - \frac{u_i(z) - u(x,y,z)}{u_H} \tag{1}$$

using the inflow wind speed u_i, the corresponding hub height value u_H and the wind speed u at the desired position. The 3DSL model is generally valid starting from a downstream distance where the pressure gradient in the stream-wise direction is negligible. Moreover, the viscous term is not considered and no external forces are applied.

Differently from other existing shear layer models, our 3DSL approach is not formulated in a polar coordinate system, but considering a Cartesian frame of reference, i.e. the stream-wise deficit u_D, the cross-stream and vertical wind components v and w are defined along the downstream x, lateral y and upward z axis respectively. In the same way as u_D, also the two latter wind components are normalised by u_H.

Considering a dimensional analysis (Cebeci and Cousteix, 2005) the steady RANS equation for flows with a shear layer along the cross-stream and vertical component can be simplified to

$$\begin{cases} \frac{\partial u_D}{\partial x} + \frac{\partial v}{\partial y} + \frac{\partial w}{\partial z} &= 0 \\ u_D\frac{\partial u_D}{\partial x} + v\frac{\partial u_D}{\partial y} + w\frac{\partial u_D}{\partial z} &= -\left(\frac{\partial \overline{u'v'}}{\partial y} + \frac{\partial \overline{u'w'}}{\partial z}\right) \\ \frac{\partial p}{\partial y} = \frac{\partial p}{\partial z} &= 0 \end{cases} \tag{2}$$

The shear stress terms on the right hand side of the second line of Eq. (2) can be modelled by means of an eddy viscosity closure introducing the eddy viscosities ϵ_y, ϵ_z and multiplying them by the corresponding cross-stream and vertical gradients of u_D:

$$\begin{aligned} \overline{u'v'} &= -\epsilon_y \frac{\partial u_D}{\partial y} \\ \overline{u'w'} &= -\epsilon_z \frac{\partial u_D}{\partial z} \end{aligned} \tag{3}$$

Further details on the eddy viscosity model are provided in Sect. 2.4.

At this point, the system of Eq. (2) is still under-determined. To balance the unknown variables and the equations, we assume that the wind components v and w define a conservative vector field in all the cross-sections $y - z$. A potential function Φ can therefore be defined such that

$$\begin{cases} \frac{\partial \Phi}{\partial y} &= v \\ \frac{\partial \Phi}{\partial z} &= w \end{cases} \tag{4}$$

Concerning multiple wakes, this assumption does not imply any limitation since a vector field resulting from the superposition of conservative vector fields is still conservative. However, this assumption limits the domain of possible solutions. For instance,

swirling wakes in which the tangential velocity is inversely proportional to the distance from the rotation axis are accepted, while wakes rotating as a rigid body are not.

The hypothesis of a potential flow is implicit in the axial symmetry imposed by Ainslie. In his model, he considers a cylindrical coordinate system defined by the radial coordinate r, the angular coordinate θ and the axial coordinate x. The corresponding velocity vector field $\overline{V}(r,\theta,x) = (v_r, v_\theta, u)$ is conservative only if $\nabla \times \overline{V} = 0$. Considering the individual cross-section planes at a certain x coordinate, it implies that $\partial v_r / \partial\theta - \partial v_\theta / \partial r = 0$. This equation is always satisfied by the Ainslie model in which the tangential velocity v_θ is neglected and the radial velocity v_r does not vary along the angular coordinate θ when a constant radial distance r is considered.

The above explanation shows that, as the 3DSL model, also the Ainslie model assumes a potential flow and therefore no vorticity on the cross-sections $y - z$. In the vortex cylinder model of the actuator disk (Burton et al., 2011), the flow field of a wind turbine wake is conservative everywhere but on the surface of the vortex cylinder which enclose the wake, along the root vortex and on the bound vortex sheet swept by the rotor blades. Accordingly, our approximation to a potential flow is reasonable for most of the simulation domain and, even if the real flow is not strictly conservative, the 3DSL model enables to find one of the solutions for the underdetermined, three dimensional shear layer problem that respects the conservation of mass and the momentum balance in the streamwise direction.

Thanks to Eq. (4) and considering that at each individual vertical cross-section $\partial u_D / \partial x$ depends only on y and z, the conservation of mass (Eq. (2), first line) can be expressed as

$$\frac{\partial^2 \Phi}{\partial y^2} + \frac{\partial^2 \Phi}{\partial z^2} = -g \tag{5}$$

where $g(y,z) = \partial u_D / \partial x$. This formulation is a second order elliptic partial differential equation of the Poisson type, which can be solved numerically.

Considering the aforementioned assumptions, the final formulation of the 3DSL model can be summarised as

$$\begin{cases} \frac{\partial^2 \Phi}{\partial y^2} + \frac{\partial^2 \Phi}{\partial z^2} & = -g \\ g & = \frac{\partial u_D}{\partial x} \\ \frac{\partial \Phi}{\partial y} & = v \\ \frac{\partial \Phi}{\partial z} & = w \\ u_D \frac{\partial u_D}{\partial x} + v \frac{\partial u_D}{\partial y} + w \frac{\partial u_D}{\partial z} & = \epsilon_y \frac{\partial^2 u_D}{\partial y^2} + \epsilon_z \frac{\partial^2 u_D}{\partial z^2} \end{cases} \tag{6}$$

2.2 The numerical implementation

The 3DSL model is implemented using finite difference schemes to obtain the numerical formulation of the physical model defined in Eq. (6). Stream-wise gradients are approximated with a forward finite difference scheme, while a central one is used for the gradient in the other directions. The solution of the wind field on each consecutive cross-section is accomplished with the following steps:

1. Approximation of the stream-wise gradient $g = \partial u_D / \partial x$ from the stream-wise momentum balance (Eq. (6), fifth line) evaluated on the previous cross-section.

2. Computation of the potential function Φ on the previous cross-section solving the Poisson equation (Eq. (6), first line)

3. Correction of v and w on the previous cross-section with the values derived from definition of Φ (Eq. (6), third and forth lines).

4. Re-iteration of the cycle from step 2 until sufficient convergence of v and w is reached.

5. Evaluation of u_D on the current section by means of numerical integration of Eq. (6, second line).

For the initial condition on the first cross-section, a disc actuator model can be applied to estimate u_D, while v and w are set to zero.

The vertical cross-sections $y - z$ are defined by a regular grid with spacing $\Delta y = \Delta z = h$; the resolution Δx along the x axis is evaluated at each cross-section. This is needed to accomplish the stability constraints of the numerical solution. In fact, the stream-wise momentum balance (Eq. (6, fifth line) is similar to the much simpler problem

$$\frac{\partial \zeta(y,z,t)}{\partial t} = \left(\frac{\partial^2 \zeta(y,z,t)}{\partial y^2} + \frac{\partial^2 \zeta(y,z,t)}{\partial z^2} \right) \mu. \tag{7}$$

The solution of this problem with a so called forward-time central-space (FTCS) finite difference scheme is numerically stable only if $\mu \Delta t / h^2 \leq \frac{1}{4}$, where Δt and $h = \Delta y = \Delta z$ are the time and space discretisation increments respectively. Inspired by this constraint, we conservatively defined the downstream step size at each cross-section as

$$\Delta x = \frac{\min(u_D) h^2}{4 \max(\epsilon_{y,z})} \tag{8}$$

.

The boundary conditions are assigned in two different ways: periodic conditions are applied to solve the Poisson equation (Eq. (6), first line), while, for the solution of the stream-wise momentum balance (Eq. (6), fifth line), u_D is set as in the initial conditions on the boundaries.

2.3 The model initialization

To run simulations with tge 3DSL model it is necessary to initialise it with the wind field at the downstream outlet of the induction zone of the rotor, i.e. the region where the pressure field is influenced by the operation of the wind turbine. In fact, as explained in Sect. 2.1 the 3DSL model is not valid in the near field behind the rotor where the pressure gradients have a major influence on the flow.

Werle (2015) and Madsen et al. (2010) suggested possible methodologies suitable for this purpose. Here, we apply a classic disk actuator approach (Burton et al., 2011) to estimate the initial wake deficit $u_{D,o}$ at the outlet of the induction zone.

We consider the stream tube depicted in Fig. 2 and defined by the cross-sections at the inlet, at the rotor and at the outlet of the induction zone. We indicate the corresponding diameters as D_i, D_r and D_o respectively. We use the same subscripts

for the section averaged wind speed U_{SA} and for the stream-wise wind component u. Following the disk actuator theory, we assume that:

- U_{SA} is homogeneous on each cross-section of the stream tube.

- The induction factor a defined by the thrust coefficient C_T as in Eq. (16) regulates the evolution of U_{SA} through the stream tube such that

$$a = 1 - \frac{U_{SA,r}}{U_{SA,i}} = \frac{1}{2}\left(1 - \frac{U_{SA,o}}{U_{SA,i}}\right) \qquad (9)$$

According to the conservation of mass of an incompressible flow across the stream tube (see Fig. 2), the following equivalences apply:

$$U_{SA,i}\,D_i^2 = U_{SA,r}\,D_r^2 = U_{SA,o}\,D_o^2 \qquad (10)$$

Replacing the induction factor in Eq. (10), it is possible to calculate the inlet and the outlet cross-section diameters of the stream tube:

$$
\begin{aligned}
D_i &= D_r\sqrt{(1-a)} \\
D_o &= D_r\sqrt{\tfrac{(1-a)}{(1-2a)}} \quad = \quad D_i\sqrt{1-2a}
\end{aligned} \qquad (11)
$$

The initial conditions $u_{D,o}$ for the 3DSL model are calculated in three steps: First, the induction factor a is homogeneously applied to the inflow wind speed u_i on the inlet cross-section of the stream tube.

$$
\begin{cases}
u_o = u_i\,(1-2a) & \text{on the inlet cross section} \\
u_o = u_i & \text{outside the inlet cross section}
\end{cases} \qquad (12)
$$

Then, the wind field is expanded according to Eq. (11). Finally, the initial deficit $u_{D,o}$ is given replacing u by u_o in Eq. (1).

To calculate the stream tube cross-sections and the corresponding average wind speeds, this method needs to be applied iteratively until convergence. In fact, the induction factor a has to be known. Usually, it can be derived from the thrust coefficient
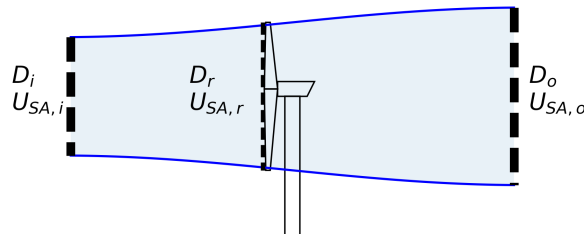
Figure 2. Sketch of the stream tube used to describe the disc actuator approach. The dashed lines represent the inflow, rotor and outlet cross-section which are indicated with the subscripts i, r, and o in the definition of the diameter and D and the section average wind speed U_{SA}.

C_T associated to the undisturbed wind speed at the inlet of the stream tube according to the wind turbine specification. In the case described here, the undisturbed wind speed is defined as average over the inlet cross-section by $U_{SA,i}$, which in turn is dependent on the induction factor a (see Eq. (11)). For this reason, an iterative process is applied starting with the rotor diameter D_r as first guess to approximate the diameter D_i of the inlet cross-section.

5   As already mentioned several times, shear layer wake models are valid only outside the induction zone. However, Madsen et al. (2010) noticed that the turbulent mixing influences the wind deficit profile already within this region. Therefore, they simulated wakes with their shear layer model starting from the rotor position. To compensate for the effect of pressure gradients not included in their model, but actually present in the reality until 2-3 rotor diameter downstream the turbine, they apply a linear filter to the ambient eddy viscosity within this range. In the same way, also the 3DSL model evaluates first the wind deficit
10 outside the induction zone to initialise the wake simulation, which in turn starts directly behind the rotor. Then, it applies the linear filter F_2 defined in Eq. (13) to the ambient eddy viscosity to mimic the effects of the pressure gradients within the near wake.

$$\begin{cases} F_2 = \frac{x/D_r}{2.5} & \text{for } 0 < x \leq 2.5 D_r \\ F_2 = 1 & \text{for } x > 2.5 D_r \end{cases} \tag{13}$$

2.4 Eddy viscosity model

15 In the 3DSL model, the eddy viscosity is evaluated as

$$\epsilon_{y,z}(x,y,z) = \frac{F_1(x)\,k\,r_{y,z}(x)\,u_{ay,z}(x,y,z)}{\Phi_m(z/L_{MO})} + \frac{F_2(x)\kappa\,u_*\,z}{\Phi_m(z/L_{MO})} \tag{14}$$

following the approach suggested by Ainslie (1988) who combined the contribution of the wake (first addend) and of the atmosphere (second addend).

    In Eq.14 we indicate the spatial dependence of the parameters, because we want to stress the fact that, thanks to the three-
20 dimensions resolved by the model, also the eddy viscosity does not need to be axisymmetric anymore and can be defined locally. For instance, it can vary linearly over the height z or depend on the local strain rates of the wind field as Sect. 2.4.1 will explain.

    The parameters describing the wake contribution to the eddy viscosity are the empirical parameter $k = 0.015$ and the filter function[1]

$$F_1 = \begin{cases} 0.65 + \left[\left(\frac{x/D_r - 4.5}{23.32}\right)^{1/3}\right] & 0 < x \leq 5.5\,D_r \\ 1 & x > 5.5\,D \end{cases} \tag{15}$$

which are included to modulate the development of the turbulence generated by the shear layer within the wake deficit (Ainslie, 1988). Last, the parameters $r_{y,z}$ and $u_{ay,z}$ are meant to represent the characteristic length and velocity scales of turbulent fluctuations within the wake.

---

[1]in Eq. 14 the rational exponent $1/3$ indicates the real cube root of the corresponding base

The parameters appearing in Eq. (14) to model the effect of the atmospheric conditions on the eddy viscosity are the momentum flux profile $\Phi_m(z_H/L_{MO})$ as function of the wind turbine hub height z_H and of the Monin-Obukonov length L_{MO} (Dyer, 1974), the Von Karman constant κ and the friction velocity u_*.

As explained in Sect. 2.3, the filter function F_2 was added following the example by Madsen et al. (2010) to compensate for
5   the pressure effect within the near wake when the 3DSL model is initialised at the rotor position.

2.4.1 Characteristic scales of turbulent fluctuations within wakes

In the 3DSL model, the characteristic turbulence length scales r_y and r_z are both approximated with a representative wake deficit radius $r(x)$ derived as a function of the normalised downstream distance x and the thrust coefficient C_T using the analytical wake model by Frandsen et al. (2006) and revised by Rathmann et al. (2006).

$$
\begin{aligned}
r(x) &= \left[\max(\beta, 0.7\, x/D_r)\right]^{0.5} \quad \text{where} \\
\beta &= \tfrac{1-a}{1-2a} \qquad\qquad\qquad \text{and} \\
a &= \tfrac{1-\sqrt{1-C_T}}{2}
\end{aligned}
\tag{16}
$$

In case of multiple wakes, only the turbine closest to the considered cross-section is regarded in the evaluation of $r(x)$ within the overlapping area.

On each cross-section, we define the local characteristic turbulence velocity scale $u_{a\,y,z}$ as a function of the position $P = (x, y, z)$. For this purpose, the local characteristic velocity scale is derived with the classic turbulence mixing length theory
15   (Pope, 2000), similarly as in the model by Keck et al. (2012). Accordingly, the turbulent velocity scales are modelled by means of the local strain rates of the wake deficit $u'_y(P) = \left.\frac{\partial u}{\partial y}\right|_P$ and $u'_z(P) = \left.\frac{\partial u}{\partial z}\right|_P$ together with the turbulence length scale approximated with $r(x)$ in the considered direction:

$$
u_{a\,y,z}(P) = u'_{y,z}(P)\, r(x)
\tag{17}
$$

2.5 Multiple wakes

20   The 3DSL model is suited for simulation of multiple wakes and does not require the addition of individual wake to resolve the wind field where wakes from different turbines are overlapping. Still, for the simulations of multiple wakes it has to deal with the definition of the inflow wind field of a wind turbine hit by other wakes. This is a delicate matter because it generates a sort of conflict between the actuator disc model used for the initialisation of the 3DSL model and the recovery of the wake within the upstream induction zone of the downstream turbine.

25   The induction zone, that is the region directly affected by the pressure gradients across the rotor, begins already in the inflow. For instance the IEC 61400-12-1 standard for power performance measurements suggests to measure the wind speed of the free inflow at least 2 rotor diameters upstream the wind turbine. Power performance measurements exclude the case of wind turbine operating in wakes. We could have followed this indication anyway, but we would have disregarded the recovery of the wake.

When a wind turbine operates within a wake, the 3DSL model uses the wind field on the rotor cross-section as the inflow in the evaluation of the section average wind speed $U_{SA,i}$. Doing this it neglects the effect of the induction zone upstream of the wind turbine, but this is necessary in order to consider the recovery of the wake. Recent studies which investigate how to model the induction zone upstream of the wind turbine rotor (Forsting et al., 2016) could provide tools to improve this pragmatic approach, but it is out of the scope of the present work.

3   Wake simulations

In this section we consider single and multiple wind turbine wakes from LES wind fields as reference to evaluate and compare results from simulations carried out with the 3DSL model and with the Ainslie model as implemented in the wind farm layout software *FLaP* (Lange et al., 2003). In the latter case we applied the square addition approach to multiple wakes.Accordingly, the local wake deficit resulting from the overlapping of the consecutive wakes is assumed as

$$u_D = 1 - \sum_i (1 - u_{D,sw_i})^2 \tag{18}$$

where u_{D,sw_i} is the deficit of the i-th single wake. The comparison includes three cases of multiple wakes (namely aligned wakes, wake-turbine and wake-wake interaction), preceded by a single wake simulation.

3.1   The test cases and the reference wind fields

All the test cases are simulated with the same atmospheric conditions and consider wakes generated with the LES simulation model implemented in PALM (Raasch and Schröter, 2001), coupled with an actuator disc model (Calaf et al., 2010) as reference. These LES wind fields deal with wakes from the Siemens SWT-3.6-120 wind turbine (120 m rotor diameter D, 90 m hub-height z_H). In the test cases two, three and four, the turbines are placed with a consecutive downstream displacement of $6\,D$ and a cumulative offset in the cross-stream direction of $0.0\,D$, $0.5\,D$ and $1.5\,D$ respectively. These layouts lead to the hub height maps of the wake deficit displayed in Fig. 3.

The wind field is evaluated on a uniform grid with a spacial resolution of 10 m ($0.083\,D$) and a total domain size of approximately 20 km, 5 km and 3.5 km along the stream-wise, cross-stream and vertical axes respectively. The reference wind field results from the temporal average of 45 min simulations with a time step close to 1 s. With a roughness length $z_0 = 0.002$ m and a vertically constant potential temperature the wind conditions should resemble a typical offshore boundary layer in neutral stratification ($\Phi_m(z_H/L_{MO}) = 1$). The friction velocity u_* evaluated fitting the logarithmic profile $u = (u_*/\kappa)\,ln(z/z_0)$ to the average vertical profile of the wind speed on the inflow section is about $0.3\mathrm{ms}^{-1}$. Under this conditions, the hub height wind speed $3.3\,D$ upstream of the first rotor is 8 ms^{-1} with 5 % turbulence intensity TI. According to this inflow wind speed, the wind turbines are operating in partial load with a thrust coefficient C_T of 0.858 (A/S).

3.2 Simulations with the shear layer models

The simulation domains of the 3DSL and of the Ainslie model were different. In the first case the cross-sections were resolved with 111 and 81 points in the lateral and vertical direction respectively, extended from $y = -7$ D to $y = +3$ D and were 8 D high. The adaptive step in the downstream direction lead to 2291 points from $x = 0$ D to $x = 20$ D. With this settings the simulation of three wind turbine wakes took about 11 s.

In *FLaP* we imposed the initial condition taking into account the turbulence intensity, the thrust coefficient and the tip speed ratio of the turbine according to Lange et al. (2003). Additionally, for test case 2 and test case 3, we considered the wake added turbulence following the empirical formula suggested by Hassan (1992) as reported in (Burton et al., 2011).

For the simulation of a single wake with *FLaP*, 181 points were considered along the downstream direction from $x = 2$ D to $x = 20$ D; the radial coordinate counted 20000 points in the range from 0 D to 7 D. The enormous amount of points in the radial direction was dictated to achieve a convergent result with a downstream step close the one of the LES wind field. This simulation setup required a computational time of about 6 s for a single wake.

3.3 The results

For a quantitative assessment of the results, we considered several virtual turbines of the same type as the one used for the simulations; their rotors are centered on the black dots printed in the wind fields of Fig. 3. An illustrative sketch of a row of the virtual turbine rotors is given in Fig. 4.

With regard to the virtual turbine rotor j, the corresponding simulation grid points i and in relation to the reference streamwise wind component u_{ref}, we analysed

 – The relative deviation of rotor average wind speed (RAWS);

$$\Delta_{RAWS, j} = \frac{\sum\limits_{i=1}^{N_j} u_i}{\sum\limits_{i=1}^{N_j} u_{ref_i}} - 1; \tag{19}$$

 – The root mean square error (RMSE)

$$E_{RMS, j} = \sqrt{\frac{\sum\limits_{i=1}^{N_j} \left(u_i - u_{ref_i}\right)^2}{N_j}}; \tag{20}$$

 – The linear regression of the streamwise wind components values on the grid points within the rotor area.

The first two figures were considered on the one hand for each virtual turbine individually. On the other hand, we calculated the overall values $\bar{\Delta}_{RAWS}$ and $\bar{E}_{RMS}$ averaging the absolute values $\Delta_{RAWS, j}$ for the former, and considering all virtual turbines at once in the calculation of the RMSE for the latter. These overall values are collected in Table 1.

The three methods of evaluation are related, but each has its own specific character. The rotor average wind speed is often used as parameter to evaluate the operational state of a wind turbine. In this sense, it is very close to the application field. However, it cannot give precise information about the accuracy of the simulated wind field because inaccurate previsions of the wake deficit could cancel out in the averaging process. The root mean square error does not suffer from this problem and

5 can express the accuracy of the simulations with more confidence. Last, we included also the regression analysis in our study because in this way we could see how well the models are correlated to the reference in terms of the coefficient of determination R^2, and of the corresponding regression line slope A and intercept B. These statistical parameters are included in Table 1 too.

To provide more information on the intermediate results of the simulations, we included figures describing the development of the horizontal and vertical profiles of the wake deficit at different cross-sections in Annex A.

Table 1. Overall performance of the 3DSL model and *FLaP* (Ainslie model) in relation to the reference large eddy simulations wind field. Namely, the average deviation $\bar{\Delta}_{RAWS}$ of the rotor average wind speed, total root mean square error $\bar{E}_{RMS}$, the coefficient of determination R^2), the corresponding regression line slope A and intercept B are included.

		Test case 1		Test case 2		Test case 3		Test case4	
		3DSL	*FLaP*	3DSL	*FLaP*	3DSL	*FLaP*	3DSL	*FLaP*
$\bar{\Delta}_{RAWS}$	$[-]$	0.20	0.20	0.17	0.23	0.17	0.38	0.17	0.29
$\bar{E}_{RMS}/u_H$	$[-]$	0.27	0.29	0.31	0.31	0.29	0.48	0.34	0.46
R^2	$[-]$	0.93	0.92	0.95	0.97	0.96	0.96	0.94	0.90
A	$[-]$	0.83	0.79	1.02	0.85	0.95	0.72	0.86	0.77
B	$[\mathrm{ms}^{-1}]$	1.31	1.57	-0.07	1.21	0.37	2.15	0.95	1.68

10 **3.3.1   Test case 1: Single wake**

In the first test case, we addressed a single wake to assess the general accuracy of the two shear layer wake models and at the same time to have a term of comparison for the simulation of multiple wakes.

Looking at the results of Fig. 5, the 3DSL model and *FLaP* tend to have fair and very similar results with values of Δ_{RAWS} (top panels) and E_{RMS}/u_H (bottom panels) below 10 % after 6 D downstream. Higher errors occur in the preceding region,

15 especially around the center of the rotor ($y = 0\ D$) where the rotor average wind speed is overestimated. Here, the 3DSL model seems to perform slightly better, in particular from the graphics of E_{RMS}. In the far wake, starting from 12 D the profiles of Δ_{RAWS} and E_{RMS} do not vary much moving downstream.

The difference between the results of the two models perceived in Δ_{RAWS} and E_{RMS}/u_H is not found in the overall rotor average wind speed $\bar{\Delta}_{RAWS}$ and in the average root mean square error $\bar{E}_{RMS}/u_H$. Similarly, the results of the regression

20 analysis are essentially the same for the two models. The corresponding scatter plots of Fig. 6 and intercept B suggests that, in general, the two models tend to overestimate the wind speed values, i.e. to underestimate the deficit.

3.3.2 Test case 2: Multiple aligned wakes

Even though the simulation of consecutive aligned wakes with the Ainslie wake model does not require the square addition approach because the wind deficit profiles remain axisymmetric, we applied this approach to be consistent with the other test cases.

The main results are collected in Fig. 7, whose top panels show that *FLaP* overestimates the rotor average wind speed Δ_{RAWS}, particularly around the axis of the real turbine rotor ($y = 0$ D) where the maximum of the deviation is reached. Moving sideways, the deviation decreases gradually.

Differently, 3SDL model underestimates the rotor average wind speed around the axis of the real turbine rotor and overestimate it around the boundaries of the wakes ($y = \pm 1$ D). Also in this case, the highest absolute deviation from the reference is around the axis of the real turbines rotor.

In general, the results give the impression that the 3DSL model simulations are a little more accurate in terms of rotor average wind speed. The same conclusion is not evident in the values of the root mean square error drawn in Fig. 7 (bottom panels). Since in both figures of merit the two models have a very similar behaviour, it is hard to draw clear conclusion from the comparison.

Contrarily from the previous test case, the overall statistics $\bar{\Delta}_{RAWS}$ and $\bar{E}_{RMS}/u_H$ sustain the impression suggested by Fig. 7: The former indicates that 3DSL simulations have a deviation from the reference in average 6 percentile points lower than *FLaP*. In contrast, the latter suggests that the two models have the same accuracy in terms of overall root mean square error.

The slope and the intercept from the regression analysis (Table 1) show that the 3DSL model approaches an almost perfect regression line. *FLaP* does not have such good results in these terms, but it is characterised by a lower spread of the data as indicated by the higher coefficient of determination R^2. This outcome can be explained with the different distribution of the deviation from the reference of the two models (see Fig. 8): The 3DSL model tends to underestimate the lower values of the wind speed, i.e. in the region around the axis of the real turbine rotor and to overestimate the higher ones. The resulting uneven distribution leads to an almost perfect regression line. Differently, *FLaP* mainly overestimates the wind speeds in their whole range causing a higher intercept and a lower slope of the regression line. The same arguments explain the results of Δ_{RAWS} described before.

Considering all the results, we conclude that the two models simulate differently the wake of this test case, but they have very similar overall performance.

3.3.3 Test case 3: Multiple wakes with 0.5 D lateral separation

The simulation of multiple wakes with offset provided more pronounced differences between the two models. Concerning the rotor average wind speed plotted in the top panel of Fig. 9, the values of Δ_{RAWS} evaluated with the 3DSL simulations are contained within ± 10 % with negative peaks around the center line of the turbines at the corresponding first downstream cross-section ($x = 8$ D, $y = -0.5$ D and $x = 14$ D, $y = -1.0$ D); otherwise the 3DSL model overestimates the Δ_{RAWS}.

The wakes predicted with *FLaP* and the square addition rule overestimate almost everywhere the rotor equivalent wind speed values and are higher than in the case of the simulation with the 3DSL model. In the results from *FLaP*, we also notice that the maximal deviation of the rotor average wind speed at each cross-section is higher than in test case 2 where the aligned wakes are supposed to be axisymmetric. Furthermore, it increases passing through the third turbine. On the contrary, we do not observe such behavior in the 3DSL model, where the maximum peaks of Δ_{RAWS} have a similar level as in test case 2 on all cross-sections. This difference between the two models might be due to the three dimensional, non axisymmetric character of the multiple wakes simulated in this test case, which is better reproducible by the 3DSL model.

Although from a different point of view, the results about the root mean square error (Fig. 9, bottom panel) lead to the same observations.

The overall statistics provide a quantitative summary of the results mentioned above; in particular, the 3DSL model achieves a deviation from the reference rotor average wind speed ($\bar{\Delta}_{RAWS}$) 11 percentile points lower than *FLaP*. Considering the overall root mean square error, the spread between the two models is even more acute: In the simulations with the 3DSL model, $\bar{E}_{RMS}$ is almost 20 percentile points lower than in *FLaP* simulations.

The regression analysis replicates here the results of test case 2, with the difference that, for the 3DSL model simulations, the slope (A) and the intercept (B) of the regression line are not so close to their ideal values 1 and 0 respectively. In turn, the coefficient of determination R^2 is little higher indicating less scatter of the data. For the simulations with *FLaP* we observe a remarkable increase in the intercept which indicates a larger overestimation of the wind speed, that means a larger underestimation of the wake deficit.

3.3.4 Test case 4: Multiple wakes with 1.5 D lateral separation

Due to the increased cross-stream separation between the three turbines considered in this test case, the flow seems composed by single wakes. The results presented in Fig. 9 are therefore comparable with those of test case 1, but with an amplified difference between the performance of the two models. In fact, with regard to the reference, both the deviation of the rotor average wind speed and the root mean square error evaluated for *FLaP* are clearly higher than the ones evaluated for the 3DSL model.

The corresponding overall values give a measure of this difference: both the deviation $\bar{\Delta}_{RAWS}$ of *FLaP* and the average root mean square error $\bar{E}_{RMS}/u_H$ are more than 10 percentile points larger than the ones of the 3DSL model.

The regression analysis provides results close to those of test case 1 for both models, a part from the intercept which reduced a little for the simulation with the 3DSL model, while it increased for *FLaP* simulations.

4 Discussion

In Sect.3.3, we compared two shear layer wake models with a different level of detail in the physical description of the flow. The results are not always easy to interpret because in some cases one model is accurate where the other is not and vice-versa. We dealt with this problem analysing different figures of merit which are generally in agreement. This temporarily solves the

conflict between the applicative point of view of the rotor average wind speed and the more wind field oriented approach of the root mean square error.

The object of comparison was the performance of the two models in the simulation of multiple wakes. In this regard, the figures of merit are generally in favour of the 3DSL model. This is a positive outcome of our research and encourage the further development of this new model. Nonetheless, the two models provided similar results for axisymmetric wakes (test case 1 and test case 2). This points out the advantage given by the third dimension resolved by the 3DSL model. In fact, in the other test cases, i.e. when multiple wakes have a lateral offset, the additional details in the physical description of the flow implemented in the 3DSL model seem to improve the results.

Despite the different performances, we found similar deficiencies in the two models. This particularly interests the flow of single wakes near to the rotor cross-section as indicated by the results of test case 1 and in test case 4. Furthermore, the regression analysis and the scatter plot indicated , the tendency to overestimate the wake deficit in the same cases. The analysis of the individual wake profiles could help to understand how to deal with this issue. In many cases, possible solution could be provided by different eddy viscosity models. In this sense, the three dimensional domain of the 3DSL model offers the possibility to develop proper spatial distributions of these quantities, while the axisymmetric two dimesional models would have more limits in the accomplishment of this task.

5   Conclusions

This paper investigates the possibility to improve the simulation of multiple wakes with engineering wake models such as the commonly used Ainslie model (Ainslie, 1988) implemented for instance in the wind farm layout software *FLaP* (Lange et al., 2003). In this regard, the paper presents a new wake shear layer model (3DSL) that can deal with non-axisymmetric flows and is therefore suitable to simulate multiple wakes at once. Differently, when the Ainslie model is applied in a wind farm, the flow of multiple wakes is evaluated superimposing the deficit of the individual wakes according to a linear or square addition approach. To allow the simulation of multiple wakes without the superposition of the individual wakes, the 3DSL model abandons the hypothesis of an axisymmetric wake assumed by Ainslie (1988) and add a third dimension to the simulation domain. In order to do this, it assumes a potential flow on the vertical cross-sections.

In a benchmark against large eddy simulations, we considered four test cases and compared wake simulations performed with *FLaP* and with the 3DSL model. The assessment was based on the average wind speed on the rotor of several fictive turbines and the corresponding root mean square error. The two models provided similar results when they simulated axisymmetric wakes, but the 3DSL model perfomed better in the test cases including non-axisymmetric wakes. In part, this might be one of the advantages of the third dimension included in the 3DSL model.

Since only few test cases using wakes simulated within large eddy simulations were addressed here, this results cannot be generalised. For the same reason we cannot make any statement about how these results could affect the estimation of the annual energy yield of a wind farm. Nevertheless, we are confident that the additional details in the physical description of

the wake flow implemented in the 3DSL model can in general offer new possibilities to improve the simulation of single and multiple wakes at an affordable computational cost.

Acknowledgements. This research was carried out in the frame of the RAVE (Research at alpha ventus) research project GW Wakes, funded by the German Federal Ministry for Economic Affairs and Energy (BMWi) based on a decision of the Parliament of the Federal Republic of Germany (grant number 0325397A). Computer resources have been partly provided by the North German Supercomputing Alliance (HLRN) and by the national research project "Parallelrechner-Cluster für CFD und WEA-Modellierung" (FKZ 0325220) funded by the Federal Ministry for Economic Affairs and Energy (BMWi). The authors further want to thank J. Schmidt and J.J. Trujillo for valuable discussions about the content of the manuscript.

References

Ainslie, J. F.: Calculating the Flowfield in the Wake of Wind Turbines, Journal of Wind Engineering and Industrial Aerodynamics, 27, 213–224, doi:10.1016/0167-6105(88)90037-2, 1988.

A/S, E. I.: windPRO 3.0.629.

5 Burton, T., Jenkins, N., Sharpe, D., and Bossanyi, E.: Wind Energy Handbook, 2nd Edition, John Wiley & Sons, Ltd., Publication, 2011.

Calaf, M., Meneveau, C., and Meyers, J.: Large eddy simulation study of fully developed wind-turbine array boundary layers, Physics of Fluids, 22, 015 110, doi:10.1063/1.3291077, 2010.

Cebeci, T. and Cousteix, J.: Three-Dimensional Incompressible Laminar and Turbulent Flows, Springer Berlin Heidelberg, 2005.

Crespo, A., Hernández, J., and Frandsen, S.: Survey of modelling methods for wind turbine wakes and wind farms, Wind Energy, 2, 1–24,

10 doi:10.1002/(SICI)1099-1824(199901/03)2:1<1::AID-WE16>3.0.CO;2-7, 1999.

Dyer, A.: A review of flux-profile relationships, Boundary-Layer Meteorology, 7, 363–372, doi:10.1007/BF00240838, 1974.

Forsting, M., Raul, A., Bechmann, A., and Troldborg, N.: A numerical study on the flow upstream of a wind turbine on complex terrain, Journal of Physics: Conference Series, 753, doi:10.1088/1742-6596/753/3/032041, 2016.

Frandsen, S., Barthelmie, R., Pryor, S., Rathmann, O., Larsen, S., Højstrup, J., and Thøgersen, M.: Analytical modelling of wind speed deficit

15 in large offshore wind farms, Wind Energy, 9, 39–53, doi:10.1002/we.189, http://dx.doi.org/10.1002/we.189, 2006.

Hassan, U.: A wind tunnel investigation of the wake structure within small wind turbine farms, E/5A/CON/5113/1890, 1992.

Katic, I., Højstrup, J., and Jensen, N. O.: A simple model for cluster efficiency, in: EWEC Proc. '86, p. 407–10, http://orbit.dtu.dk/fedora/objects/orbit:66401/datastreams/file_f7da8eb2-e49c-4dc9-9ee5-72846f40ef34/content, 1986.

Keck, R.-E., Veldkamp, D., Madsen, H. A., and Larsen, G.: Implementation of a Mixing Length Turbulence Formulation into the Dynamic

20 Wake Meandering Model, Journal of Solar Energy Engineering, 134, 021 012–021 012, doi:10.1115/1.4006038, 2012.

Lange, B., Waldl, H.-P., Guerrero, A. G., Heinemann, D., and Barthelmie, R. J.: Modelling of Offshore Wind Turbine Wakes with the Wind Farm Program FLaP, Wind Energy, 6, 87–104, doi:10.1002/we.84, 2003.

Lissaman, P. B. S.: Energy effectiveness of arbitrary arrays of wind turbines, Journal of Energy, 3, 323–328, doi:10.2514/3.62441, 1979.

Machefaux, E.: Multiple Turbine Wakes, Ph.D. thesis, Technical University of Denmark, 2015.

25 Madsen, H. A., Larsen, G. C., Larsen, T. J., Troldborg, N., and Mikkelsen, R.: Calibration and Validation of the Dynamic Wake Meandering Model for Implementation in an Aeroelastic Code, Journal of Solar Energy Engineering, 132, 041 014–041 014, doi:10.1115/1.4002555, 2010.

Pope, S.: Turbulent Flows, Cambridge University Press, 2000.

Raasch, S. and Schröter, M.: PALM - A large-eddy simulation model performing on massively parallel computers, Meteorologische

30 Zeitschrift, 10, 363–372, doi:10.1127/0941-2948/2001/0010-0363, 2001.

Rathmann, O., Barthelmie, R., and Frandsen, S.: Turbine Wake Model for Wind Resource Software, in: EWEC, https://www.researchgate.net/profile/R_Barthelmie/publication/268300272_Turbine_Wake_Model_for_Wind_Resource_Software/links/561d248208aec7945a252a37.pdf?inViewer=0&pdfJsDownload=0&origin=publication_detail, 2006.

Vermeer, L, J., Sørsen, J, N., and Crespo, A.: Wind turbine wake aerodynamics, Progress in Aerospace Science, 39, 467–510, 2003.

35 Walker, K., Adams, N., Gribben, B., Gellatly, B., Nygaard, N. G., Henderson, A., Marchante Jimémez, M., Schmidt, S. R., Rodriguez Ruiz, J., Paredes, D., Harrington, G., Connell, N., Peronne, O., Cordoba, M., Housley, P., Cussons, R., Håkansson, M., Knauer, A., and Maguire, E.:

An evaluation of the predictive accuracy of wake effects models for offshore wind farms, Wind Energy, 19, 979–996, doi:10.1002/we.1871, 2016.

Werle, M. J.: Another engineering wake model variant for horizontal axis wind turbines, Wind Energy, pp. 279–299, doi:10.1002/we.1832, 2015.

5   Appendix A: Wake deficit profiles

The comparison of the 3DLS model and of *FLaP* with the reference wind field from large eddy simulations (LES) reported in this paper deals with figure of merits representative for integral results, i.e. they can hardly reveal the actual output of the two models. For this reason we show in this annex the downstream development of the wake deficit for the test cases analysed in this paper.
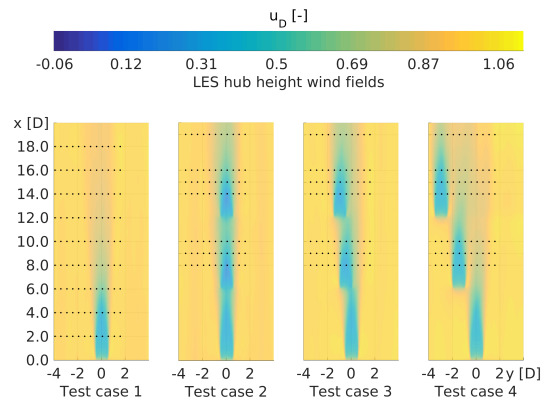
Figure 3. Colour map of the hub height wake deficit u_D evaluated for the test cases from the large eddy simulations (LES).
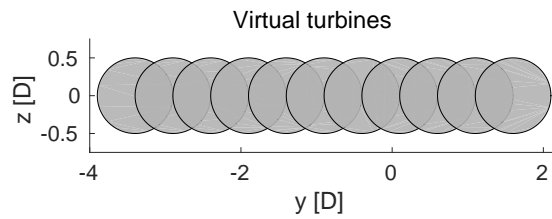
Figure 4. Illustrative sketch of the rotors of the virtual turbines considered to assess the performance of the engineering models in relation to the large eddy simulations.
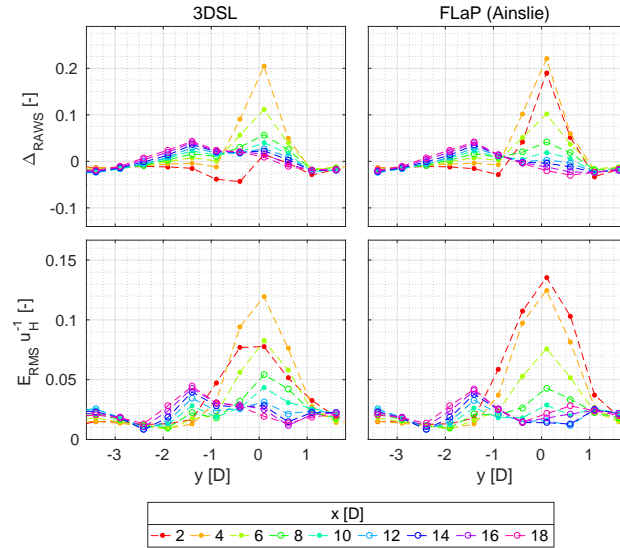
Figure 5. Test case 1 (Single wake). Deviation of the rotor average wind speed Δ_{RAWS} (top panels) and of the root mean square error E_{RMS} (bottom panels) evaluated in relation to the large eddy simulations wind field for the simulation with the 3DSL model and with *FLaP*.
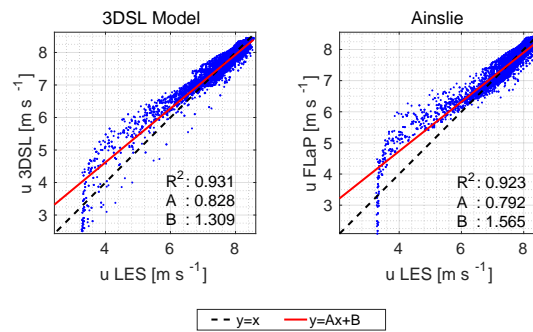
Figure 6. Test case 1 (Single wake). Scatter plot and corresponding regression line of the wind speed derived from the 3DSL model (left) and from the *FLaP* wake simulations in relation to the reference wind field calculated with large eddy simulations (LES).
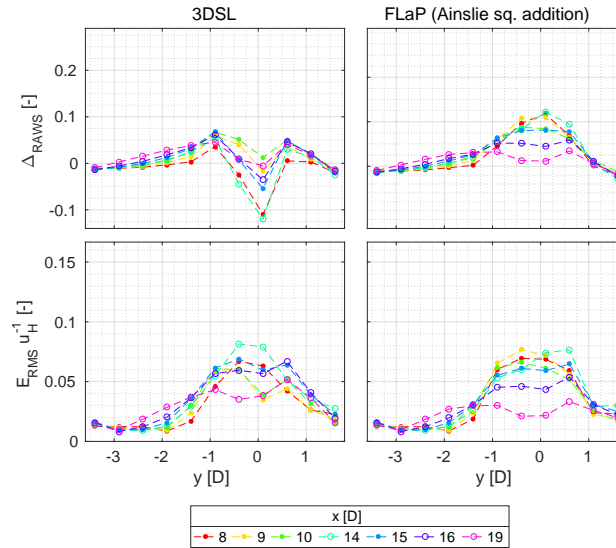
Figure 7. Test case 2 (Multiple aligned wakes). Deviation of the rotor average wind speed Δ_{RAWS} (top panels) and of the root mean square error E_{RMS}/u_H (bottom panels) evaluated in relation to the large eddy simulations wind field for the simulation with the 3DSL model and with *FLaP*.
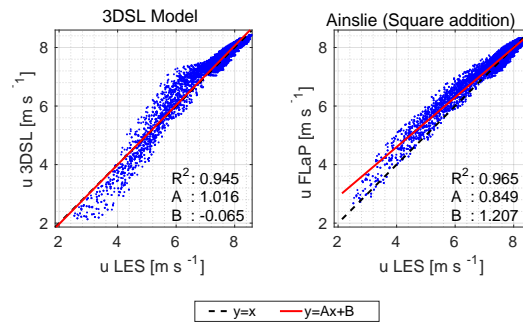
Figure 8. Test case 2 (Multiple aligned wakes) Scatter plot and corresponding regression line of the wind speed derived from the 3DSL model (left) and from the *FLaP* wake simulations in relation to the reference wind field calculated with large eddy simulations (LES).
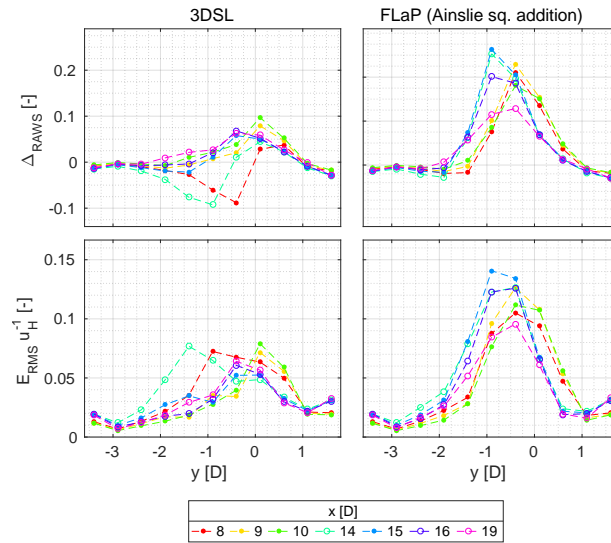
Figure 9. Test case 3 (Multiple wakes with 0.5 D later offset). Deviation of the rotor average wind speed Δ_{RAWS} (top panels) and of the root mean square error E_{RMS} (bottom panels) evaluated in relation to the large eddy simulations wind field for the simulation with the 3DSL model and with *FLaP*.
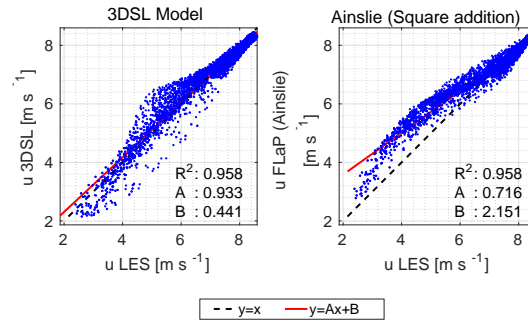
Figure 10. Test case 3 (Multiple wakes with a 0.5 D lateral separation). Scatter plot and corresponding regression line of the wind speed derived from the 3DSL model (left) and from the *FLaP* wake simulations in relation to the reference wind field calculated with large eddy simulations (LES).
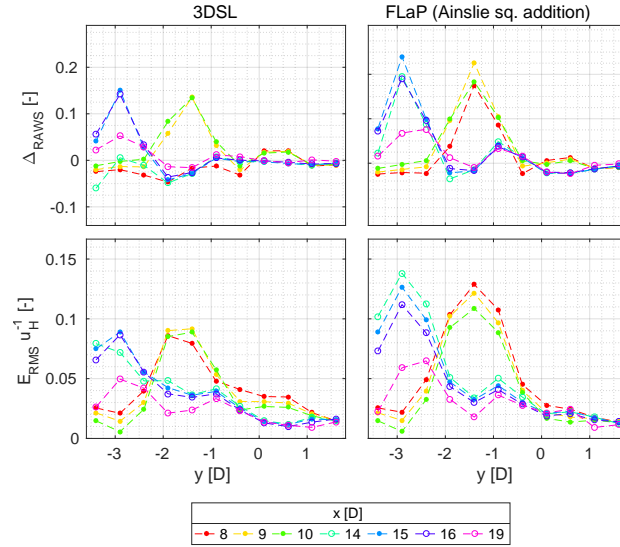
Figure 11. Test case 4 (Multiple wakes with 1.5 D later offset). Deviation of the rotor average wind speed Δ_{RAWS} (top panels) and of the root mean square error E_{RMS} (bottom panels) evaluated in relation to the large eddy simulations wind field for the simulation with the 3DSL model and with *FLaP*.
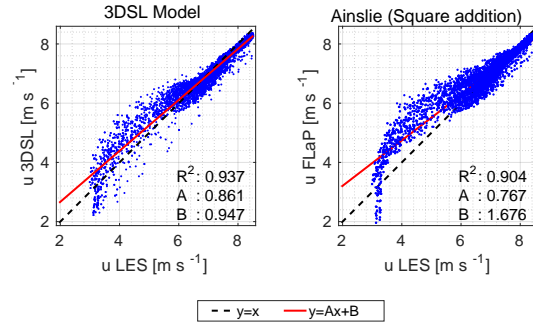
Figure 12. Test case 4 (Multiple wakes with a 1.5 D lateral separation). Scatter plot and corresponding regression line of the wind speed derived from the 3DSL model (left) and from the *FLaP* wake simulations in relation to the reference wind field calculated with large eddy simulations (LES).
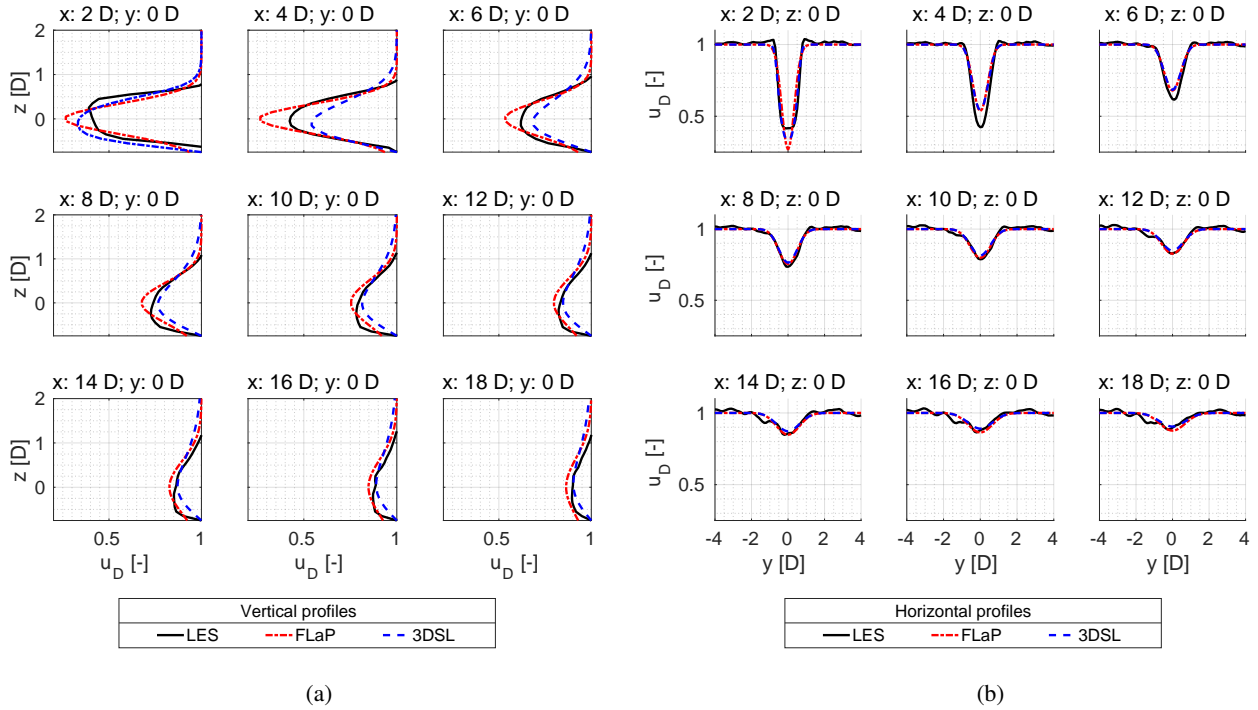
Figure A1. Test case 1 (Single wake). Downstream development of the vertical (a) and horizontal (b) profiles of the wake deficit evaluated along the wind turbine rotor axis from the 3DSL model and from the *FLaP* simulations and from the reference large eddy simulation (LES) wind field.
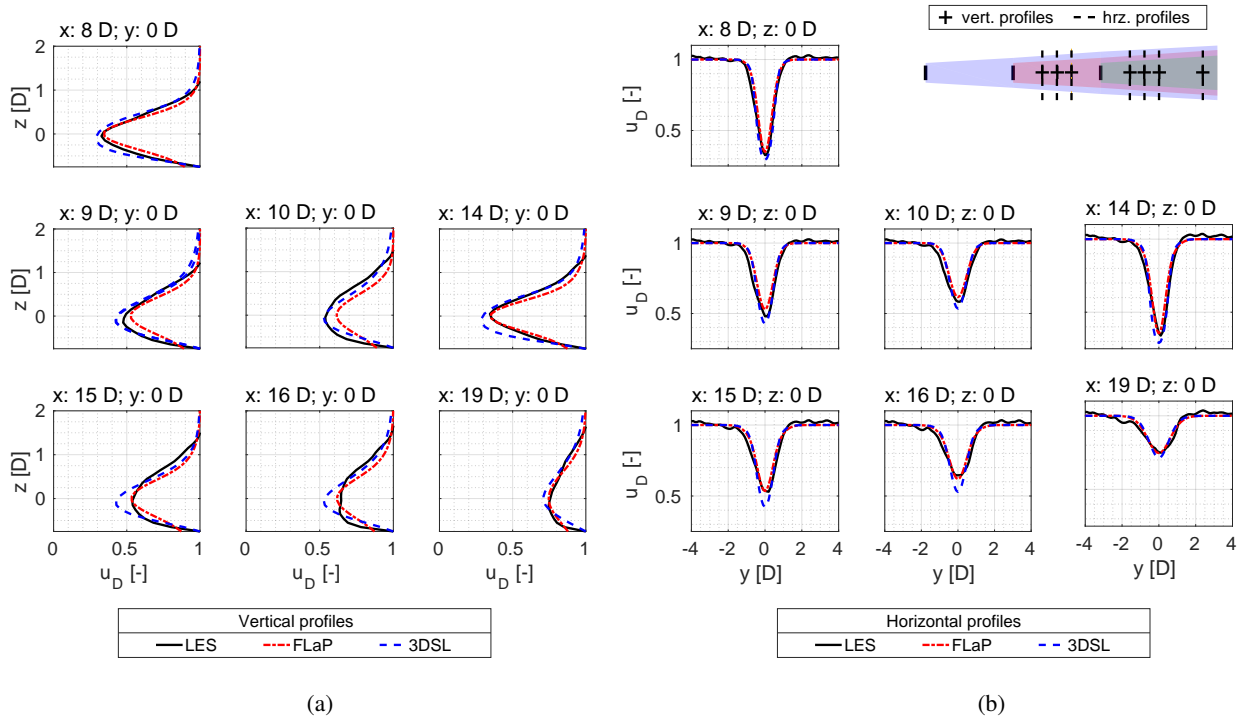
Figure A2. Test case 2 (Multiple aligned wakes) Downstream development of the vertical (a) and horizontal (b) profiles of the wake deficit evaluated along the common axis of the wind turbines from the 3DSL model and *FLaP* simulations and from the reference large eddy simulations (LES) wind field. The position of the considered profiles is illustrated in top-right corner of (b).
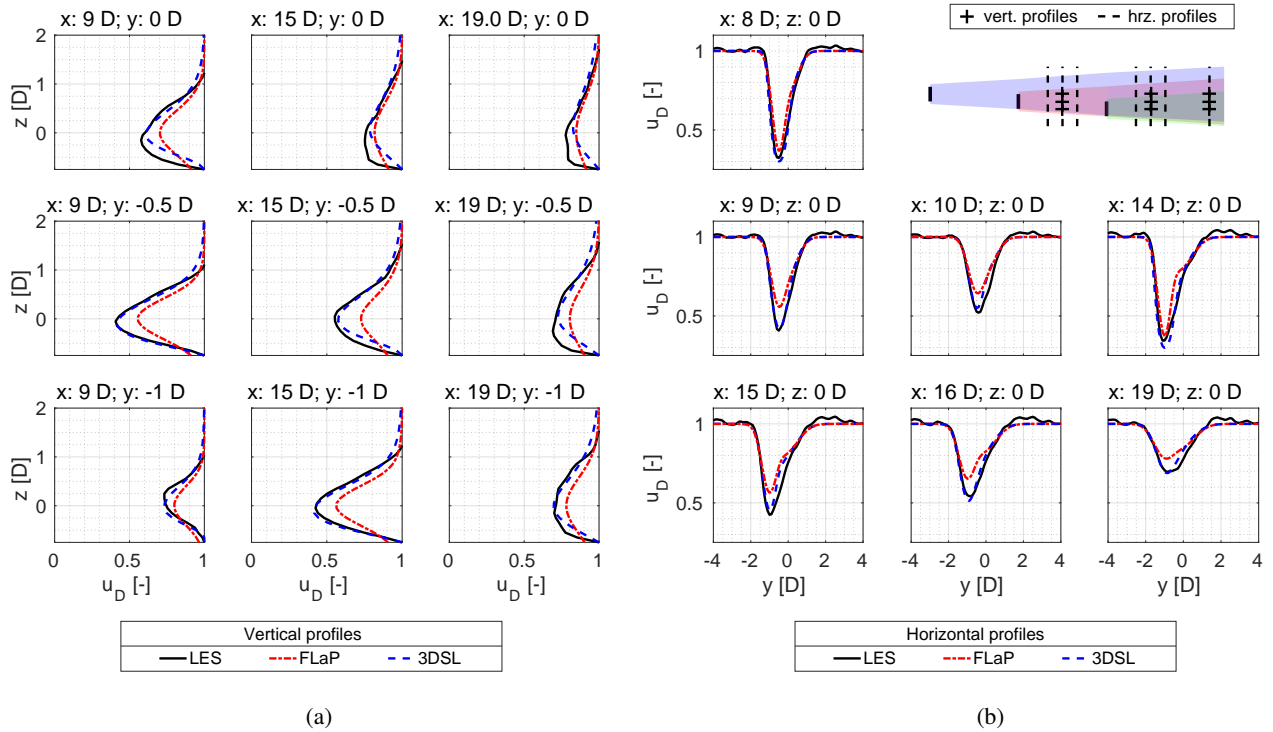
Figure A3. Test case 3 (Multiple wakes with 0.5 D lateral separation). Downstream development of the vertical (a) and horizontal (b) profiles of the wake deficit evaluated along the common axis of the wind turbines from the 3DSL model and *FLaP* simulations and from the reference large eddy simulations (LES) wind field. The position of the considered profiles is illustrated in top-right corner of (b).
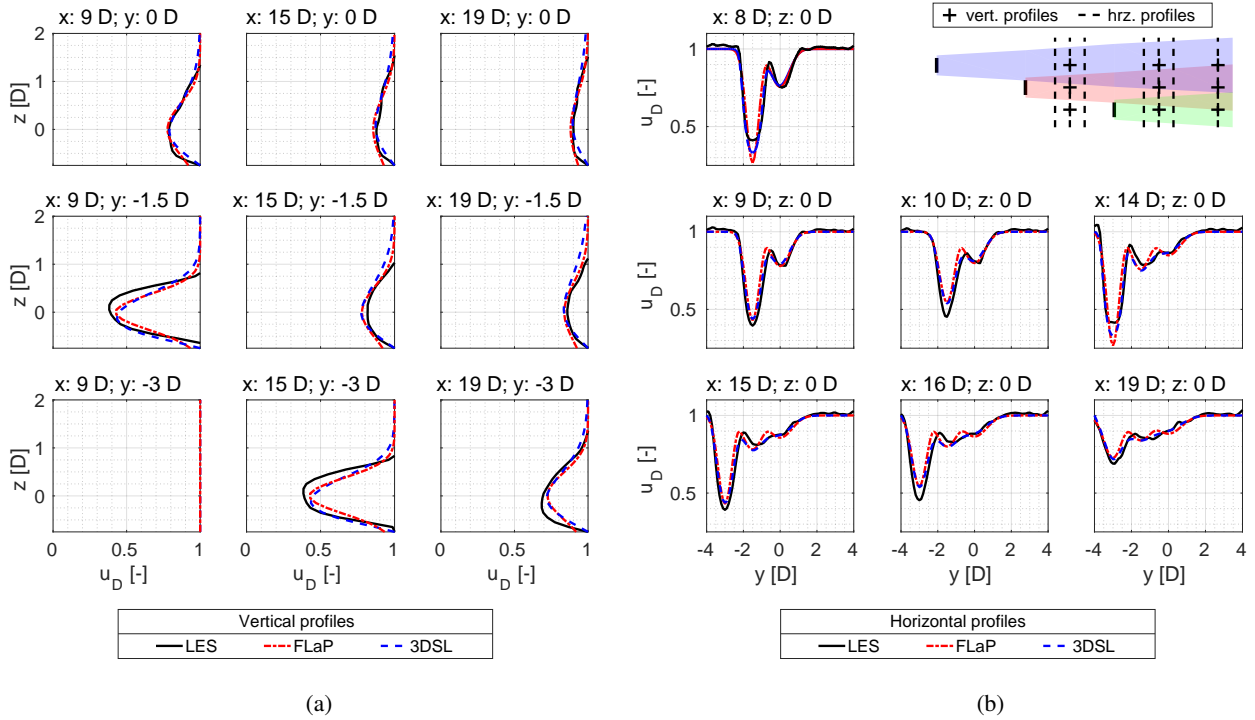
Figure A4. Test case 4 (Multiple wakes with 1.5 D lateral separation). Downstream development of the vertical (a) and horizontal (b) profiles of the wake deficit evaluated along the common axis of the wind turbines from the 3DSL model and *FLaP* simulations and from the reference large eddy simulations (LES) wind field. The position of the considered profiles is illustrated in top-right corner of (b).